Generalization of Iterative RestorationTechniques for Super-Resolution

Marcia L. S. Aguena, Nelson D. A. Mascarenhas
Departamento de Computação
UFSCar - Universidade Federal de São Carlos
São Carlos, SP - Brazil
Email: {aguena, nelson}@dc.ufscar.br

***Abstract*—The resolution enhancement of an image is always desirable, for almost all situations, but mainly if the image has the purpose of visual analysis. The hardware development for increasing the image resolution at its capture still has a higher cost than the algorithm solutions for super-resolution (SR). Like image restoration, super-resolution is also an ill-conditioned inverse problem. This work analyses the iterative restoration methods (Van Cittert, Tikhonov-Miller and Conjugate Gradient) which propose solutions for the ill-conditioning problem and compares them with the IBP method (Iterative Back Projection) proposed by Irani-Peleg [1] and Komatsu et al. [2]. The analysis of the found similarities is the basis of a generalization, that other iterative restoration methods can have their properties adapted, such as regularization of the ill-conditioning, noise reduction and other degradations and the increase of the convergence rate can be incorporated to the techniques of super-resolution.**

***Keywords*-super-resolution, image restoration; iterative restoration, iterative back-projection.**

I. Introduction

The search of higher resolution images comes from two major purposes: to improve pictorial information for human interpretation and preprocessing information for automatic procedures, such as segmentation, classification or recognition. The super-resolution (SR) objective is to obtain a higher resolution image from low resolution ones. The application of SR techniques cover a wide range of purposes, from surveillance and radar to telescope and microscope images. Nowadays, with the popularization of high resolution TV, the SR techniques are used as a part of decoded images. In general terms, the strategy that characterizes SR comprises three major steps:

1) *Low Resolution Image acquirement*: A sequence of Low Resolution (LR) images is obtained from one scene with geometric non-integer displacements between images, two by two (considering a pixel as unit distance).
2) *Registration or Motion Compensation*: The geometric transformations are estimated to fit the LR acquired images to the High Resolution (HR) spatial grid of the desired result.
3) *HR Image Reconstruction*: The reconstruction problem solution is found from images obtained by previous step. The research of this paper is concentrated in this step.

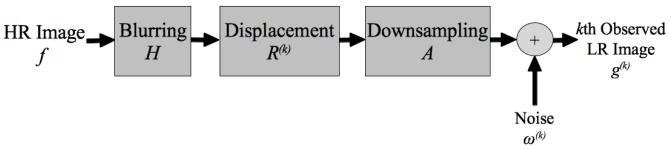

Fig. 1. Block diagram of SR image degradation process.

The SR formation model can be represented by the block diagram of Fig. 1.

The degradation process responsible for the kth LR image can be described as:

$$g^{(k)} = AHR^{(k)}f + \omega^{(k)}, \qquad \forall k = 1, 2, \cdots, K \tag{1}$$

where A is the downsampling matrix, H the blurring matrix, $R^{(k)}$ the displacement from kth LR image, $g^{(k)}$ the lexicographic representation of kth observed LR image and f is the lexicographic representation of the HR image.

Choosing matrices $D^{(k)}$ in the way to represent the blurring, displacement and downsampling, such as $D^{(k)} = HR^{(k)}A$, (1) can be rewritten as [3], [4]:

$$g^{(k)} = D^{(k)}f + \omega^{(k)}, \qquad \forall k = 1, 2, \cdots, K \tag{2}$$

The system described by (2) is an ill-conditioned inverse problem and as such kind of problem, the iterative solution must be regularized.

A. Related work

The SR research field started with Huang and Tsay [5] seminal work and since then has spread considerably. Approaches using Frequency Domain [6], [7], [8], Bayesian [3], Example-Based [9], [10], [11], [12], Set Theoretic [13], [14] and Interpolation [15] have been applied to SR techniques. The research arm that supports this paper starts with Keren and Peleg [16] work exploring sub pixel displacement of LR images to get a HR image and laid the foundation of further work of Irani and Peleg.

The method developed by Irani and Peleg [1] obtained HR images with a technique similar to the back-projection reconstruction method used in computer-aided tomography. Each HR image pixel is a sum of different projections of the

same LR image area, determined by the image blurring and displacement. Komatsu et al [2], in a similar way, adapted this same method on LR images obtained from different sensors with different aperture cameras, in other words, different lattices(either uniform or not) to create a HR image over a uniform pixel distribution.

Bannore [15], also based on [1], used several interpolation methods to incorporate different characteristics to the IBP method and evaluated the results.

B. Technique overview

The central point of this work is to adapt image restoration techniques to SR, and can be reached by analysing the similarities between the Van Cittert with Reblurring restoration method and the Iterative Back Projection (IBP) SR method. The generalization of these similarities (section II-C) enables to adapt other restoration techniques (Tikhonov-Miller and Conjugate Gradient) for SR and create new methods that incorporate regularization features to SR - as ringing artifact reduction methods incorporated in section V . From the positive results obtained, we suggest that other adaptations can be made to create new super resolution methods. Beyond the obtained results, this paper opens up the possibility to apply other restoration techniques to the SR problem.

II. Drawing an Analogy between Irani-Peleg and Van Cittert with Reblurring

A. Irani-Peleg IBP Method

The Irani-Peleg SR method can be divided in two parts. The first one is to generate a HR image from LR image projections, and can be represented algebraically by (3):

$$f_{i+1} = f_i + c\sum_{k=1}^{n}(D_{BP}^{(k)})^2(g^{(k)} - g_i^{(k)}) \tag{3}$$

The term $(D_{BP}^{(k)})^2$ is the back-projection matrix that creates a projection from the difference $(g^{(k)} - g_i^{(k)})$ in a HR image and c is a normalizing constant.

The second part of the IBP method is to obtain the LR images from imaging process simulation, and can be represented by equation (4):

$$g_i^{(k)} = D_{PSF}^{(k)} f_i \tag{4}$$

where $D_{PSF}^{(k)}$ is the matrix that extracts de value of each pixel in $g_i^{(k)}$ from the area in f_i that influences then.

The choice of D_{BP} is not unique and can be done arbitrarily, unlike $D_{PSF}^{(k)}$ which represents a sensor characteristic. According to the authors, a good choice is $(D_{BP}^{(k)})^2 = D_{PSF}^{(k)}$, if $D_{PSF}^{(k)}$ is symmetric and real.

Taking an initial guess of f_0 as a sum of $g^{(k)}$ projections, the entire method can be described by:

$$\begin{aligned} \hat{f}_0 &= c\sum_{k=1}^{n}(D_{BP}^{(k)})^2 g^{(k)} \\ \hat{f}_{i+1} &= c\sum_{k=1}^{n}(D_{BP}^{(k)})^2(g^{(k)} - D_{PSF}^{(k)} f_i) \end{aligned} \tag{5}$$

In order to compensate for the fact that noise is ignored in (5), when the step represented by (1) is done, the highest and the lowest discrepant values of each $g_i^{(k)}$ pixel are discharged, providing in this way a some sort of regularization to noise amplification.

B. Van Cittert with Reblurring

The following framework can represent the restoration problem: g, the image to be restored, can be represented by blurring (H) and noise (ω) over an image f [17], [18], [19] in the following way:

$$g = Hf + \omega \tag{6}$$

One of the iterative solutions of (6) applies a reblurring matrix over Van Cittert iteration as [17]:

$$\begin{aligned} \hat{f}_0 &= 0 \\ \hat{f}_{i+1} &= \hat{f}_k + \beta H^t(g - H\hat{f}_k) \end{aligned} \tag{7}$$

According to [17], the method converges if:

$$0 < \beta < \frac{2}{|\lambda_{max}|^2} \tag{8}$$

where λ_{max} is the largest eigenvalue of H. We must observe that $\lambda_{max} \neq 0$ is a requirement, in other words, H must be invertible. It is easy to verify that if (8) converges, the limiting solution is the inverse filter.

C. Similarities

There is a clear resemblance between the restoration problem, represented by (6) and a SR problem, represented by (2). Therefore, it is no surprise that an analogy between the pair (1), (2) and (7) for iterative methods can be drawn. It is easy to see that if we find a symmetric matrix D_i capable of performing the role of D_{PSF} in (2), D_t can do the same for D_{BP} and the Irani-Peleg/Van Cittert matrix formulation for SR will be given by:

$$\begin{aligned} \hat{f}_0 &= c\sum_{k=1}^{n}(D^{(k)})^t g^{(k)} \\ \hat{f}_{i+1} &= f_i + \beta c\sum_{k=1}^{n}(D^{(k)})^t(g^{(k)} - D^{(k)} f_i) \end{aligned} \tag{9}$$

If a is the rate of up-sampling and n is the quantity of images used in the process, the normalized constant c can be given by:

$$c = \frac{a^2}{n} \tag{10}$$

Another adjustment that is made in (10) consists of incorporating the relaxation parameter β to control the convergence speed.

D. IBP/Van Cittert Matrix Formulation for SR Algorithm

The method represented by (9) can be described by the following algorithm steps:

1) *Generating the initial guess*: $\hat{f}_0$ is obtained by the sum of the initial LR images properly oversampled, registered and deblurred.
2) *Simulating Imaging Process*: The n LR images $\hat{g}_i^{(k)}$ are obtained almost like a inverse process of previous step: blurring, registering and subsampling $\hat{f}_i$ (The terms $\hat{g}_i^{(k)}$ can be defined as $D^{(k)} f_i$ and were suppressed in (9) for simplification).
3) *Calculating the Back-Projection Contributions*: The BP contributions of each image is the diference between the observed LR image $g^{(k)}$ and the simulated LR image $\hat{g}_i^{(k)}$.
4) *Applying the Back-Projection Contributions on the Estimated HR Image*: Each BP contribution is added to the last estimated HR image $\hat{f}_i$.
5) *Repeat to Convergence*: Repeat the steps 2 to 4 until convergence of $\hat{f}_i$.

Fig. 2 represents graphically the described algorithm:

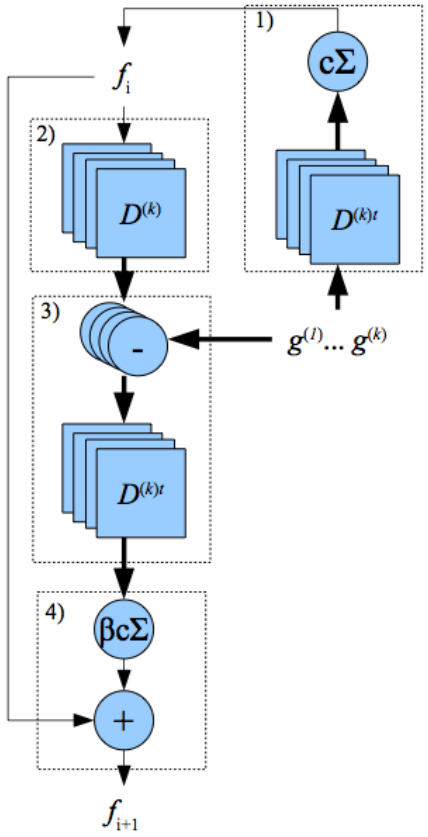

Fig. 2. Block diagram of IBP/Van Cittert matrix formulation for SR algorithm.

III. Adaptation of Tikhonov-Miller Restoration Method

A. Tikhonov-Miller Restoration

A possible regularization form of (7) is given by Tikhonov-Miller and can be represented by:

$$\hat{f} = (H^t H + \alpha C^t C)^{-1} H^t g \tag{11}$$

with C and α the regularization matrix and coefficient, respectively.

Observe that, when $\alpha \to 0$, (11) is identical to (7). We can also notice that matrix D acts as a low pass filter and matrix C as a high pass filter. For the iterative version of (11) we have:

$$\begin{aligned} \hat{f}_0 &= \beta H^t g \\ \hat{f}_{i+1} &= \hat{f} + \beta((H^t H + \alpha C^t C)\hat{f}_i - H^t g) \\ &= (I - \alpha\beta C^t C)\hat{f}_i + \beta H^t (g - H\hat{f}_i) \end{aligned} \tag{12}$$

If $\alpha = 0$, (12) is equal to (7).
The iteration will converge if:

$$0 < \beta < \frac{2}{|\lambda_{max}|} \tag{13}$$

where λ_{max} is the largest eigenvalue of $(H^t H + \alpha C^t C)$.

B. Tikhonov-Miller Super-Resolution (TMSR)

Following the generalization developed in section II-C, the SR form of (12) is given by:

$$\begin{aligned} \hat{f}_0 &= c\sum_{k=1}^{n} (D^{(k)})^t g^{(k)} \\ \hat{f}_{i+1} &= (I - \alpha\beta C^t C) f_i \\ &+ \beta c \sum_{k=1}^{n} (D^{(k)})^t (g^{(k)} - D^{(k)} f_i) \end{aligned} \tag{14}$$

This adaptation goal is the robust regularization incorporated to control the noise amplification, a very helpful tool when the number of LR images available is small and the situation cannot afford to discharge any calculated pixel of $g_i^{(k)} = D^{(k)} f_i$ as proposed in IBP method.

C. TMSR Algorithm

The method represented by (14) is very similar to the one described in section II-D, only the regularization part is embedded:

1) *Generating the initial guess*: $\hat{f}_0$ is obtained by the sum of the initial LR images properly oversampled, registered and deblurred.

2) *Simulating Imaging Process*: The n LR images $\hat{g}_i^{(k)}$ are obtained almost like an inverse process of previous step: blurring, registering and subsampling $\hat{f}_i$.
3) *Calculating the Back-Projection Contributions*: The BP contributions of each image is the diference between the observed LR image $g^{(k)}$ and the simulated LR image $\hat{g}_i^{(k)}$.
4) *Regularizing the Estimated HR Image*: Multiplying the estimated HR image $\hat{f}_i$ by the matrix $(I - \alpha\beta C^t C)$.
5) *Applying the Back-Projection Contributions on the Regularized Estimated HR Image*: Each BP contribution is added to the last regularized estimated HR image $\hat{f}_i$.
6) *Repeat to Convergence*: repeat the steps 2 to 5 until convergence of $\hat{f}_i$.

Fig. 3 represents graphically the described algorithm:

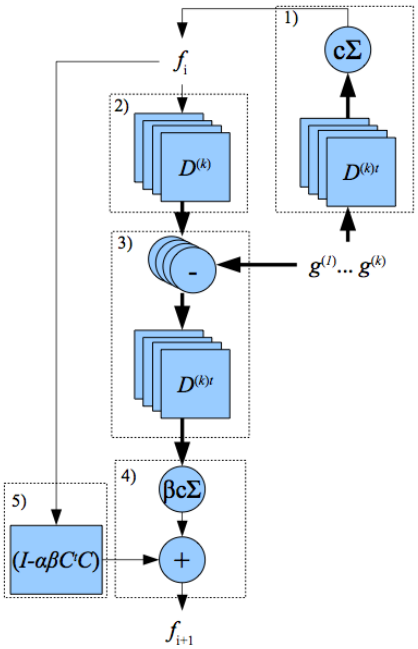

Fig. 3. Block diagram of TMSR algorithm.

IV. Adaptation of Conjugate Gradient Restoration Method

A. Conjugate Gradient Restoration

This method has been successfully used in optimization theory to reach a faster convergence. The basic form of the algorithm is given by:

$$\begin{aligned} r_i &= -(H^t H + \alpha C^t C)\hat{f}_i + H^t g \\ p_i &= r_i + \gamma_i p_{i+1} \\ \hat{f}_{i+1} &= \hat{f} + \beta_i p_i \end{aligned} \tag{15}$$

The term r_i is the steepest descent direction and γ_i is a weight coefficient. At each iteration $\hat{f}_i$ is updated by a product of γ_i and r_i in the direction of p_i.

The optimal value for γ_i and β_i are given by:

$$\gamma_i = \frac{||r_i||^2}{||r_{i-1}||^2} \tag{16}$$

$$\beta_i = \frac{r_i^t p_i}{||Dp_i||^2 + \alpha||Cp_i||^2} \tag{17}$$

For $\gamma_i \to 0$ the iteration (15) becomes (12).

B. Conjugate Gradient Super-Resolution (CGSR)

The algorithm implementation for SR can be described as:

$$\begin{aligned} r_i &= -c\sum_{k=1}^{n}(D^{(k)t}D^{(k)} + \alpha C^t C)\hat{f}_i + D^{(k)t}g^{(k)} \\ p_i &= r_i + \gamma_i p_{i+1} \\ \hat{f}_{i+1} &= \hat{f}_i + \beta_i p_i \end{aligned} \tag{18}$$

The optimized values of γ_i and β_i are:

$$\gamma_i = \frac{||r_i||^2}{||r_{i-1}||^2} \tag{19}$$

$$\beta_i = \frac{r_i^t p_i}{||(c\sum_{k=1}^{n} D^{(k)})p_i||^2 + \alpha||Cp_i||^2} \tag{20}$$

This method brings the same advantages as TMSR associated with a fast convergence.

C. Algorithm of CGSR

Although the Conjugated Gradient and Tikhonov-Miller algorithm for restoration have the same idea, the algebraic formulation of the equations (18), (19) and (20) masks the structure of the algorithms described in sections II-D and III-C, so the algorithm will be described in a different way:

1) *Generating the initial guess*: $\hat{f}_0$ is obtained by the sum of the initial LR images properly oversampled, registered and deblurred.
2) *Calculating* r_i.
3) *Calculating* γ_i.
4) *Calculating* p_i.
5) *Calculating* β_i.
6) *Calculating* f_{i+1}.
7) *Repeat steps 2 to 6 until convergence*.

Fig. 4 represents graphically the described algorithm:

V. Ringing Artifact Reduction

The use of regularization to stabilize the inversion of the ill-conditioned matrix D usually causes a regularization error that can be recognized as ringing and others artifacts. Lagendijk and Biemond [17] proposed an adaptive constrained iterative restoration method, including two diagonal matrices S and R such as:

$$\hat{f} = (H^t I_R H + \alpha C^t I_S C)^{-1} H^t I_R g \tag{21}$$

where I_S and R are diagonal matrices composed by the coefficients:

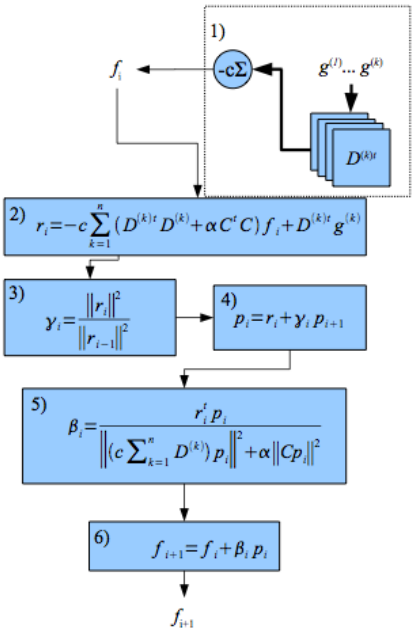

Fig. 4. Block diagram of CGSR algorithm.

$$s_{ij} = \frac{1}{1+\mu \max\left[0, \sigma_g^2 - \sigma_\omega^2\right]} \quad (22)$$

$$r_{ij} = \frac{1}{1+(\mu \max\left[0, \sigma_g^2 - \sigma_\omega^2\right])^{-1}} \quad (23)$$

σ_g^2 is the local variance around $g(i,j)$ pixel and σ_ω^2 the variance of the whole image g. Incorporating this restriction on TMSR, we have:

$$\begin{aligned} \hat{f}_0 &= c\sum_{k=1}^{n}(D^{(k)})^t I_R g^{(k)} \\ \hat{f}_{i+1} &= (I - \alpha\beta C^t I_S C) f_i \\ &+ \beta c \sum_{k=1}^{n}(D^{(k)})^t I_R (g^{(k)} - D^{(k)} f_i) \end{aligned} \quad (24)$$

For CGSR:

$$\begin{aligned} r_i &= -c\sum_{k=1}^{n}(D^{(k)t} I_R D^{(k)} + \alpha C^t I_S C)\hat{f}_i + D^{(k)t} I_R g^{(k)} \\ p_i &= r_i + \gamma_i p_{i+1} \\ \hat{f}_{i+1} &= \hat{f}_i + \beta_i p_i \end{aligned} \quad (25)$$

The optimized values of β and γ are:

$$\gamma_i = \frac{||r_i||_R^2}{||r_{i-1}||_R^2} \quad (26)$$

$$\beta_i = \frac{r_i^t p_i}{||(c\sum_{k=1}^{n} D^{(k)})p_i||_R^2 + \alpha||Cp_i||_S^2} \quad (27)$$

where the operation $||\cdot||_Q^2$ is the weighted l-2 norm with q_{ij} coeficients of diagonal matrix I_Q.

VI. Experiment

The algorithms were implemented in Matlab and tested with four 128x128 pixels images LR images synthesized from 256x256 Lena image (Fig. 5(a)). The choice of work with synthetic images is due to the fact that to work with real images it would be necessary to tackle the problem of blur identification and precise registration, and that is not the focus of this work. The final result is very dependent on the correct parametrization of blur and registration. So for better comparison among the methods, the results obtained from synthetic images were selected.

In all methods the Laplacian operator was chosen for C, given in the spatial domain as:

$$C = \begin{bmatrix} 0.00 & -0.25 & 0.00 \\ -0.25 & 1.00 & -0.25 \\ 0.00 & -0.25 & 0.00 \end{bmatrix} \quad (28)$$

Although the matrix representation of the SR problem is elegant and clean, the size of the matrices D and C are quite worrying. Fortunately the matrices are sparse and the Matlab has functions to deal with this case.

For the first experiment, the original image was blurred (defocussing with radius R=2 pixels), displaced (0.25 pixel in four different directions), downsampled (with 2 factor), and added noise (zero mean and standard deviation $sd = 0.0316$) to produce the LR images (Fig. 5(b)).

(a) (b)

Fig. 5. (a) original image (256x256 pixels); (b) one of four synthetic observed images (128x128 pixels), downsampled (factor 0.5), with defocussing blur (R=2) and noise (standard deviation=0.0316), shown zoomed 2x.

To simulate the IBP method, TMSR was applied with $\beta = 1$, $\alpha = 0$ (Fig. 6(a)). The difference between this simulation and the real IBP is that no discard was made to minimize the noise.

The TMSR (Fig. 7) and CGSR (Fig. 8) methods were tested with (a) and without (b) adaptive constraints. Is interesting to notice that, in the constrained adaptive iteration image, there is a noise reduction only in the smooth areas, but not near the edges, in an attempt to preserve the contrast characteristics of the observed images.

Fig. 6. (a) IBP result simulated by TMSR with $\beta = 1$, $\alpha = 0$.

(a) (b)

Fig. 7. (a) TMSR with $\beta = 1$, $\alpha = 0.5$; (b) TMSR with adaptive constraints, $\beta = 1$, $\alpha = 0.5$ and $\mu = 100$. .

The graphic on Fig. 9 shows the behavior of ISNR for each method. Although the TMSR results are better than CGSR method, CGSR reaches the convergence significantly faster than TMSR.

The second experiment differs from the first in blur size (R=4) and almost no noise (zero mean and standard deviation $SD = 0.0032$) to generate the inicial LR images (Fig. 10). We can observe how noise destabilize the presented methods comparing this and previous results.

With less noise and a larger blurring, is possible to observe better the ringing artifact (Fig. 11, Fig. 12(a) and Fig. 13(a)). On there conditions the IBP works better but the method does not converge.

(a) (b)

Fig. 8. (a) CGSR with $\beta = 1$, $\alpha = 0.125$; (b) CGSR with adaptive constraints, $\beta = 1$, $\alpha = 0.125$ and $\mu = 100$.

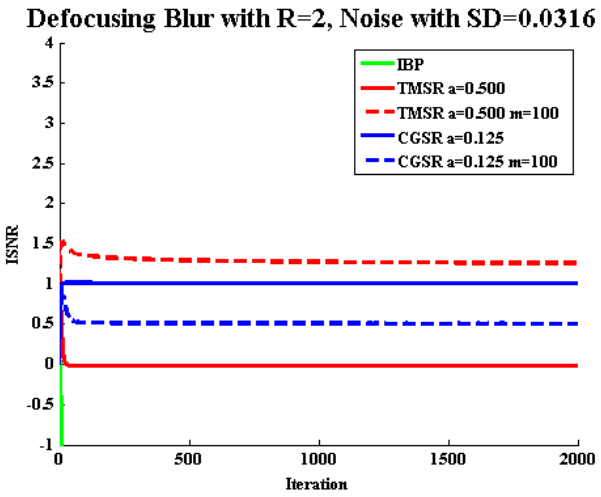

Fig. 9. Comparative graphic of the ISNR behavior of the tested methods

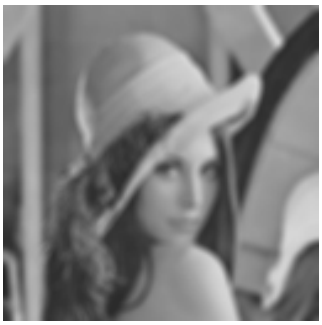

Fig. 10. One of four synthetic observed images (128x128 pixels), downsampled (factor 0.5), with defocussing blur (R=4) and noise (standard deviation=0.0032) zoomed 2x.

Fig. 11. IBP result simulated by TMSR with $\beta = 1$, $\alpha = 0$

The third experiment (Fig. 8 and Fig. 9) differs from the first in blur (motion with 8 pixels in a $\pi/4$ angle) and almost no noise (zero mean and standard deviation $sd = 0.0032$) (Fig. 15).

Is interesting to observe that when the blur kernel is larger, the ringing problem and also the effect of the constrained

(a) (b)

Fig. 12. (a) TMSR with $\beta = 1$, $\alpha = 0.125$; (b) TMSR with adaptive constraints, $\beta = 1$, $\alpha = 0.125$ and $\mu = 100$. .

(a) (b)

Fig. 13. (a) CGSR with $\beta = 1$, $\alpha = 0.125$; (b) CGSR with adaptive constraints, $\beta = 1$, $\alpha = 0.125$ and $\mu = 100$.

adaptive iterations method become more evident.

VII. Results and Discussion

This work presents an interpretation of Irani-Peleg and Komatsu et al SR methods as a super- resolution adaptation of Van-Cittert iterative restoration method. The generalization is made by inserting in the iterations projections of registered LR images in a similar way to the back-projection of CAT image reconstruction, in the restoration iterations. This strategy is exploited in a Tikhonov-Miller adaptation for SR proposal method and in a constrained adaptive iterative restoration method for ringing reduction as well. The proof that this generalization is possible opens up a range of new super-resolution approaches using well known and tested iterative restoration methods to improve SR methods such as Higher Convergence Order and POCS, for instance.

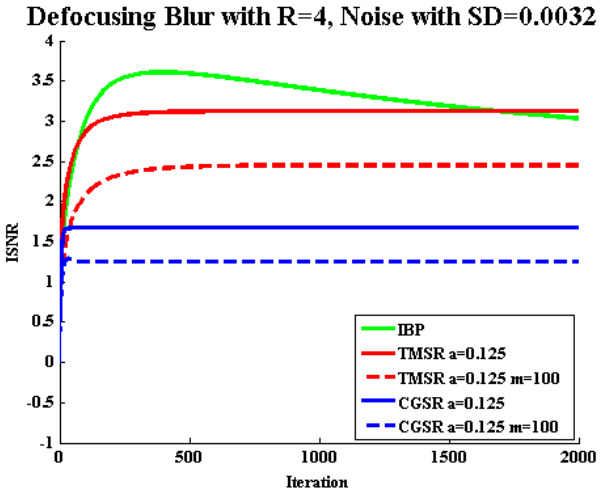

Fig. 14. Comparative graphic of the ISNR behavior of the tested methods

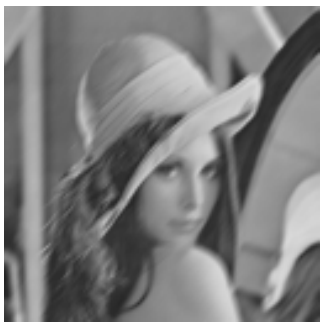

(a)

Fig. 15. One of four synthetic observed images (128x128 pixels), down-sampled (factor 0.5), with defocussing blur (R=4) and noise (standard deviation=0.0032) zoomed 2x.

(a)

Fig. 16. (a) IBP result simulated by TMSR with $\beta = 1$, $\alpha = 0$

(a) (b)

Fig. 17. (a) TMSR with $\beta = 1$, $\alpha = 0.5$; (b) TMSR with adaptive constraints, $\beta = 1$, $\alpha = 0.5$ and $\mu = 100$. .

(a) (b)

Fig. 18. (a) CGSR with $\beta = 1$, $\alpha = 0.125$; (b) CGSR with adaptive constraints, $\beta = 1$, $\alpha = 0.125$ and $\mu = 100$.

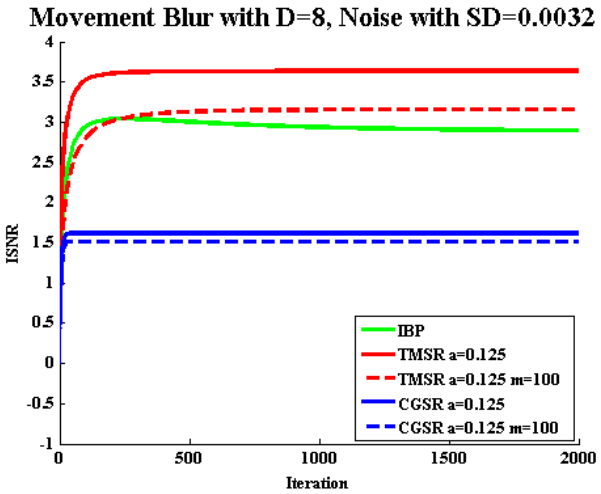

Fig. 19. Comparative graphic of the ISNR behavior of the tested methods

ACKNOWLEDGMENT

The authors would like to thank CAPES for Marcia L.S. Aguena student scholarship.

REFERENCES

[1] M. Irani and S. Peleg, "Super resolution from image sequence," in *Proceedings of 10th International Conference on Pattern Recognition (ICPR)*, 1990, p. 120.

[2] K. A. T. Komatsu, T. Igarashi and T. Saito, "Very high resolution imaging scheme with multiple different-aperture cameras," *Signal Processing: Image Communication*, vol. 5, no. 5-6, pp. 511 – 526, 1993, special Issue on Digital High Definition Television.

[3] R. M. A.K. Katsaggelos and J. Mateos, *Super resolution of images and video*, ser. Synthesis Lectures on Image, Video, and Multimedia Processing. Morgan Claypool, 2007.

[4] J. Yang and T. S. Huang, "Image super-resolution: historical overview and future challenges," in *Super-resolution imaging*, P. Milanfar, Ed. CRC Press, 2010, pp. 20–34.

[5] T. S. Huang and R. Y. Tsay, "Multiple frame image restoration and registration," in *Advances in Computer Vision and Image Processing*, vol. 1. Greenwich: JAI, 1984, pp. 317–339.

[6] H. C. K. N. K. Bose and H. M. Valenzuela, "Recursive total least squares algorithm for image reconstruction from noisy, undersampled frames," *Multidimensional Syst. Signal Process.*, vol. 4, pp. 253–268, July 1993.

[7] S. P. Kim and W. Su, "Recursive high-resolution reconstruction of blurred multiframe images," *IEEE Transactions on Image Processing*, vol. 2, pp. 534–539, 1993.

[8] W. Yu-Su and S. P. Kim, "High-resolution restoration of dynamic image sequences," *International Journal of Imaging Systems and Technology*, vol. 5, no. 4, pp. 330–339, 1994.

[9] D. Capel and A. Zisserman, "Computer vision applied to super resolution," *IEEE Signal Processing Magazine*, vol. 20, no. 3, pp. 75–86, 2003.

[10] T. R. J. W. T. Freeman and E. C. Pasztor, "Example-based super-resolution," *IEEE Comput. Graph. Appl.*, vol. 22, pp. 56–65, March 2002.

[11] S. Baker and T. Kanade, "Limits on super-resolution and how to break them," *IEEE Transactions on Pattern Analysis and Machine Intelligence*, vol. 24, no. 1, pp. 1167 – 1183, September 2002.

[12] T. H. J. Yang, J. Wright and Y. Ma, "Image super-resolution via sparse representation," to appear in *IEEE Transactions on Image Processing*, 2010, preprint: http://perception.csl.uiuc.edu/ jnwright/Yang10-TIP.pdf.

[13] A. M. Tekalp, M. K. Ozkan, and M. I. Sezan, "High-resolution image reconstruction from lower-resolution image sequences and space varying image restoration," in *In: Proc. IEEE Int. Conf. Acoustics, Speech and Signal Processing (ICASSP*, 1992, pp. 169–172.

[14] M. I. S. A. J. Patti and A. M. Tekalp, "Super resolution video reconstruction with arbitrary sampling lattices and non-zero aperture time," *IEEE Trans. Image Processing*, no. 8, 1997.

[15] V. Bannore, *Iterative-interpolation super-resolution image reconstruction: a computationally efficient technique*, 1st ed. Springer Publishing Company, Incorporated, 2009.

[16] S. P. D. Keren and R. Brada, "Image sequence enhancement using sub-pixel displacements," in *In Proc. Computer Vision and Pattern Recognition*, 1988, pp. 742–746.

[17] R. L. Lagendijk and J. Biemond, *Iterative identification and restoration of images*. Secaucus, NJ, USA: Springer-Verlag New York, Inc., 2001.

[18] M. Bertero and P. Boccacci, *Introduction to inverse problems in imaging*. Institute of Physics Publishing, 1998.

[19] J. Kaipio and E. Somersalo, *Statistical and computational inverse problems (applied mathematical sciences) (v. 160)*, 1st ed. Springer, dec 2004.